Highly confined guiding of terahertz surface plasmon polaritons on structured metal surfaces

C. R. WILLIAMS[1], S. R. ANDREWS[1], S. A. MAIER[2]*, A. I. FERNÁNDEZ-DOMÍNGUEZ[3], L. MARTÍN-MORENO[4] AND F. J. GARCÍA-VIDAL[3]*

[1]Department of Physics, University of Bath, Bath BA2 7AY, UK
[2]Experimental Solid State Group, Physics Department, Imperial College, London SW7 2AZ, UK
[3]Departamento de Física Teórica de la Materia Condensada, Universidad Autónoma de Madrid, E-28049 Madrid, Spain
[4]Departamento de Física de la Materia Condensada, Facultad de Ciencias-ICMA, Universidad de Zaragoza-CSIC, E-50009 Zaragoza, Spain
*e-mail: S.Maier@imperial.ac.uk; fj.garcia@uam.es

Published online: 3 February 2008; doi:10.1038/nphoton.2007.301

Metamaterials are artificial materials with subwavelength structure[1] that enable the translation of magnetic[2] and electric responses[3] into spectral regions not accessible through naturally occurring materials. Here, we report direct measurements of the propagation and confinement of terahertz electromagnetic surface modes tightly bound to flat plasmonic metamaterials that consist of metal surfaces decorated with two-dimensional arrays of subwavelength-periodicity pits. These modes are surface plasmon polaritons with an effective plasma frequency controlled entirely by the surface geometry[4]. The mode spectrum and penetration depth into air demonstrate strong wavelength-scale energy confinement to the surface below the electromagnetic band edge; this is in stark contrast to the very weak confinement found at flat metal surfaces in this spectral regime. The results are in good agreement with analytical and numerical models of surface plasmon polaritons propagating on structured perfect-conductor surfaces, and imply that plasmonic metamaterials could help miniaturize optical components or lead to improved chemical or biochemical sensors.

Since the late 1980s the development of highly sensitive, coherent spectroscopic tools in the far infrared, particularly in the so-called 'terahertz gap' between 0.1 THz and 3 THz, has led to many applications in this previously under-used spectral window. Examples include the study of electronic coherence in semiconductors[5], dielectric characterization of a wide range of materials[6] and pharmaceutical quality control[7]. Sensing applications[8,9], particularly in security and genetic testing, often require the detection of minute quantities of material. In such cases it is desirable to tightly confine the probing radiation, while at the same time providing easy accessibility of the guided mode. This is difficult at THz frequencies, where the wavelengths are of the order of hundreds of micrometres. Various approaches have been suggested, including stripline resonators[8], parallel-plate waveguides[10] and coupled photonic-crystal resonators[11]. Here, we describe investigations of high-confinement THz guiding on plasmonic metamaterials.

Coupling between light and the collective oscillations of the electron plasma at a metal–dielectric interface gives rise to surface plasmon polaritons (SPPs)[12]. At frequencies close to the intrinsic plasma frequency, which for metals generally lies in the UV region, SPPs exhibit subwavelength field decay. Such modes have found applications in magneto–optic data storage, chemical sensing, near-field microscopy and spectroscopy, biomedical applications[13] and miniaturized photonic circuits[14,15]. At lower frequencies, in the far-infrared and microwave regions, conductors also support electromagnetic (EM) surface waves, but here metals resemble perfect conductors and the fields are only weakly confined in the dielectric. Such extended surface EM modes, known as Sommerfeld or Zenneck waves, have recently been studied at THz frequencies[16–18].

Plasmonic metamaterials based on metals offer a potentially more versatile approach to engineering tightly confined surface modes in the THz regime than semiconductors, which can be doped to obtain plasma frequencies in the THz range[19], or high-index dielectric overlayers on flat metallic films. This is due to the fact that SPP dispersion and spatial confinement can be controlled by means of surface patterning. Any metal surface structure, such as arrays of holes or grooves, increases the binding of surface waves, as discussed by Goubau[20] and Mills and Maradudin[21]. Physically, this arises because indentations lead to greater penetration of the field into the metal in an effective-medium model. Even in an extremely thin metal sheet, perforation with an array of holes leads to the appearance of confined surface modes[22]. More recently, the concept was extended[4] with the introduction of the idea of versatile plasmonic metamaterials consisting of metal surfaces textured with subwavelength-scale corrugations or dimples and that have surface waves that mimic the properties of SPPs (dubbed 'spoof' SPPs) even in the perfect-conductor limit. The existence of such SPPs has recently been indirectly verified using microwave reflectivity measurements[23]. In this Letter, we directly observe SPP propagation on this class of metamaterials and demonstrate their strong localization to the surface at THz frequencies in a manner quantitatively consistent with theoretical predictions.

We have studied SPP propagation on two planar copper surfaces (I and II) perforated by square arrays of square, copper-lined holes (Fig. 1a and inset in Fig. 2; see Methods for

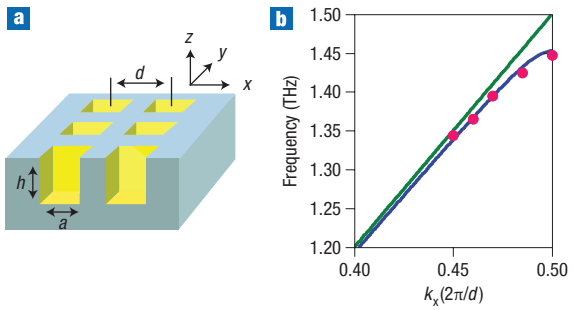

Figure 1 Plasmonic metamaterial geometries under study. **a**, Schematic of the plasmonic metamaterial showing holes in yellow. **b**, SPP dispersion curve for sample II near the Brillouin zone boundary. The green curve indicates the light line, the blue curve shows the MEA calculation, and red points indicate the FDTD calculation.

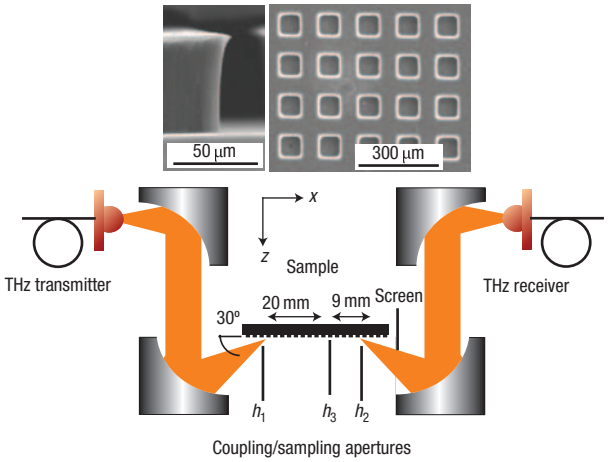

Figure 2 Schematic of the experimental arrangement to study SPP propagation. Insets show electron micrographs of the top and cleaved edges of sample I.

dimensions). Figure 1b shows the dispersion relation (angular frequency ω versus propagation constant k_x) for sample II calculated using a quasi-analytical modal expansion approximation (MEA)[24], which takes diffraction into account up to the tenth order, and its verification by finite-difference time-domain (FDTD) simulations[25]. As is apparent, the SPP dispersion curve (blue) deviates from the light line (green) as the zone boundary at $k_x = \pi/d$, where d is the period, is approached, although an asymptotic region cannot be reached for air-filled holes.

The metamaterials were studied experimentally using THz time-domain spectroscopy, in which the coherently detected signal current at a particular frequency is proportional to the THz electric field. Coupling of p-polarized free-space radiation to SPPs was achieved using an aperture of wavelength-scale width h_1, defined by a steel razor blade perpendicular to the sample

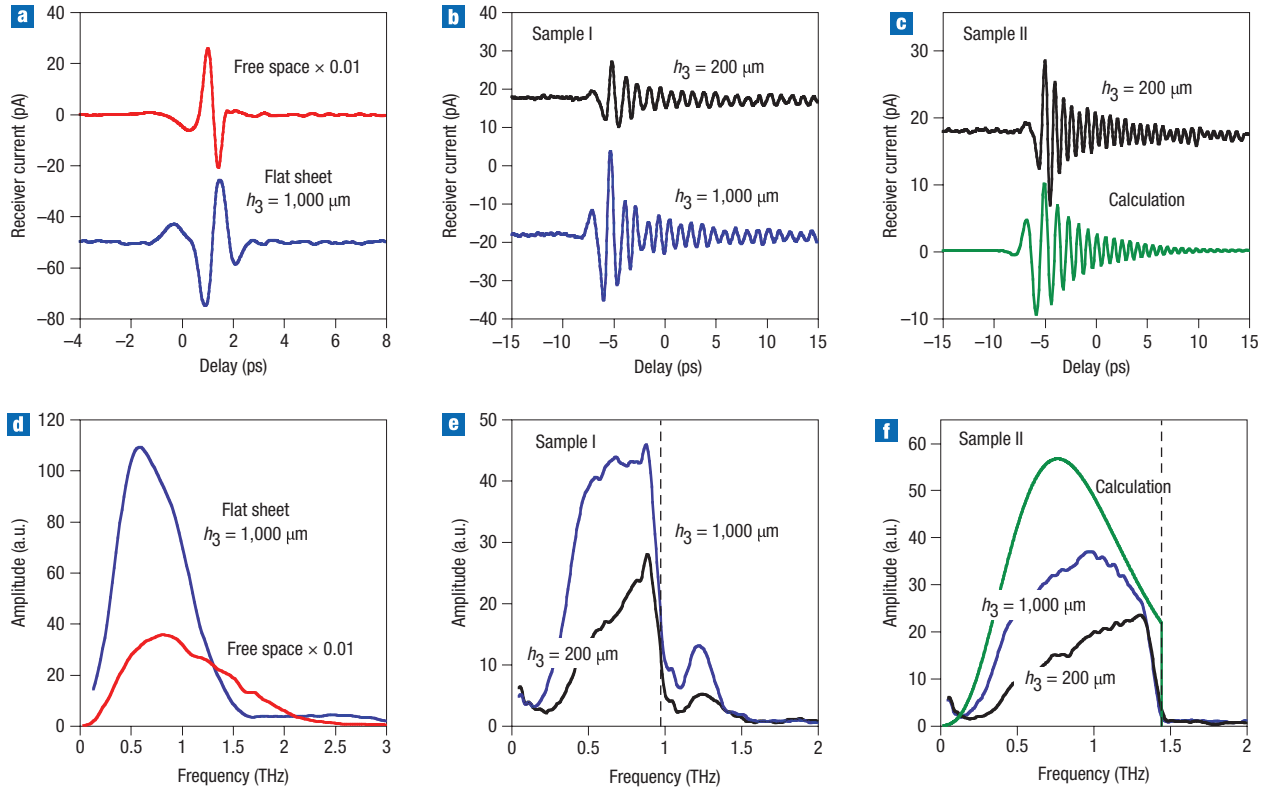

Figure 3 THz signals and their spectra. **a**–**c** Signals and **d**–**f** spectra for different arrangements. Free-space coupling of the transmitter and receiver and propagation on a flat sheet (**a**,**d**) sample I (**b**,**e**), sample II (**c**, **f**). Panels **c** and **f** also show a calculation of the effect of SPP dispersion on pulse shape. The dashed vertical lines in **e** and **f** indicate the zone boundaries.

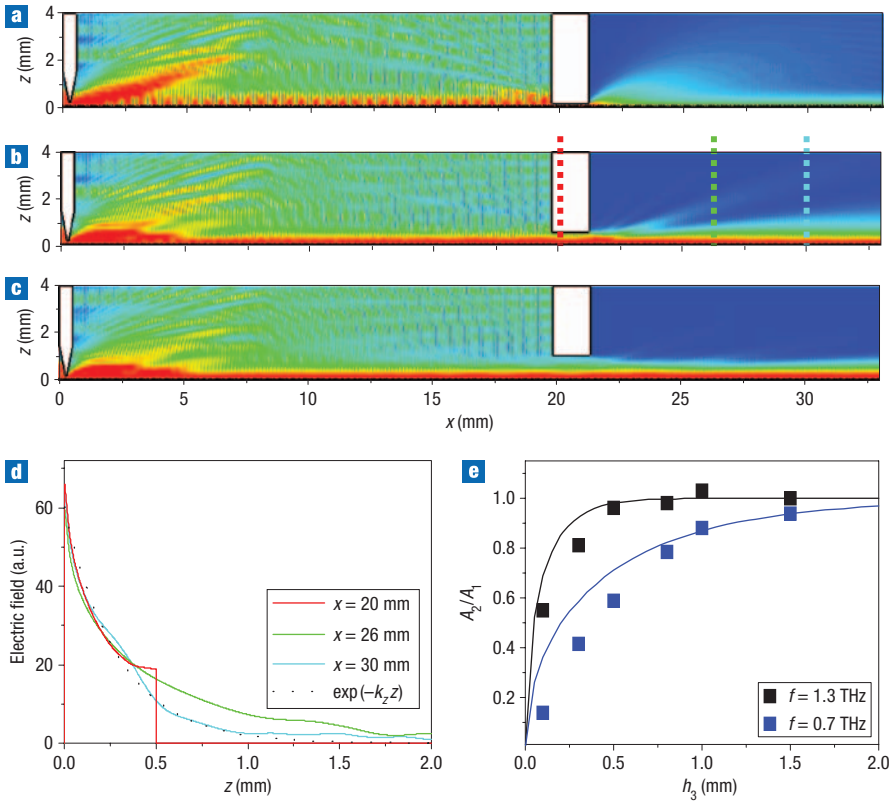

Figure 4 Numerical simulations of spoof SPP propagation. a–c, Simulated absolute-electric-field maps for sample II at an SPP frequency of 1.3 THz for $h_3 = 0.1$ mm (**a**), $h_3 = 0.5$ mm (**b**) and $h_3 = 1.0$ mm (**c**). Red colour indicates high field and blue indicates low field. **d**, Field profiles along z at the positions indicated by the dotted lines in panel **b**.The dotted curve in **d** shows the profile predicted using the MEA. **e**, Ratio A_2/A_1 as a function of h_3 for two different frequencies, $f = 1.3$ THz (black) and $f = 0.7$ THz (blue). Points correspond to values obtained from FIT and full lines are obtained using equation (1) and the MEA.

surface[16], as shown in Fig. 2. Diffraction at the aperture allows phase matching to the slower SPP. An intermediate aperture (h_3) made from a 1.5-mm-thick aluminium sheet is used to probe the extent of the SPP field along z, as described below, and diffraction at the final razor blade (aperture h_2) is used to transform the SPP back into free-space radiation for detection. It is important to appreciate that the propagation distance after the excitation region for the modal shape of the surface wave to be fully developed is governed by the perpendicular amplitude decay length, $l_z = 1/\mathrm{Im}(k_z)$ with $k_z^2 = \omega^2/c^2 - k_x^2$, which makes observations of Zenneck waves on flat surfaces difficult[18] (l_z is $\sim$10 cm for copper at 1 THz). In the metamaterial case, l_z is a few millimetres or less over a large frequency range near the band edge, and therefore the SPP waves are fully developed in our set-up, as verified in the EM simulations described below.

Figure 3 shows time-domain signals and their spectra after propagation along the two sample surfaces (Fig. 3b,c,d,f). It also shows, for comparison, data obtained by direct free-space coupling of the THz transmitter and receiver (that is, no sample) and for propagation on a perfectly flat copper surface (Fig. 3a,d). The time-domain trace of the featureless surface is similar to that obtained with no sample. Because of the extremely low dispersion of the Zenneck wave on a flat surface, the small change in shape is mainly due to the filtering effect of the apertures[13]. In contrast, the signals from the metamaterials show pronounced ringing, which persists for more than 10 ps, and the spectra exhibit sharp cut-offs at frequencies close to those of the Brillouin zone boundaries indicated by the vertical bars in Fig. 3e and f. Figure 3c and f also shows a calculated time-domain trace and spectrum for sample II. The calculation includes model functions for the electric field produced by the transmitter and for the receiver response[26], which together reproduce the free-space signal and spectrum in Fig. 3a and d. The propagation of the SPP between the in- and out-coupling apertures is calculated using, for simplicity, a first-order approximation to the MEA (ref. 24) and neglecting the transmission functions of the apertures. The good qualitative agreement with the experimental shape of the THz pulse shows that the propagation is mainly determined by the slowing down of the SPP near the band edge.

If we assume that the intermediate razor blade simply passes part of the incident SPP without significantly altering its field distribution, then, to a first approximation, the effect is to integrate the Poynting vector parallel to the surface. Energy conservation then requires that the ratio of the transmitted and incident fields, $A_2(\omega)$ and $A_1(\omega)$ respectively, on either side of the aperture is given by

$$A_2(\omega)/A_1(\omega) = \sqrt{1 - \exp(-2\,k_z h_3)} \qquad (1)$$

The detected field after out-coupling, $E(\omega)$, is proportional to $A_2(\omega)$ if diffraction by the aperture can be neglected, so that k_z can, in principle, be determined from the variation of $E(\omega)$ with h_3. To test the above assumptions we performed numerical simulations of the SPP propagation using the finite-integration

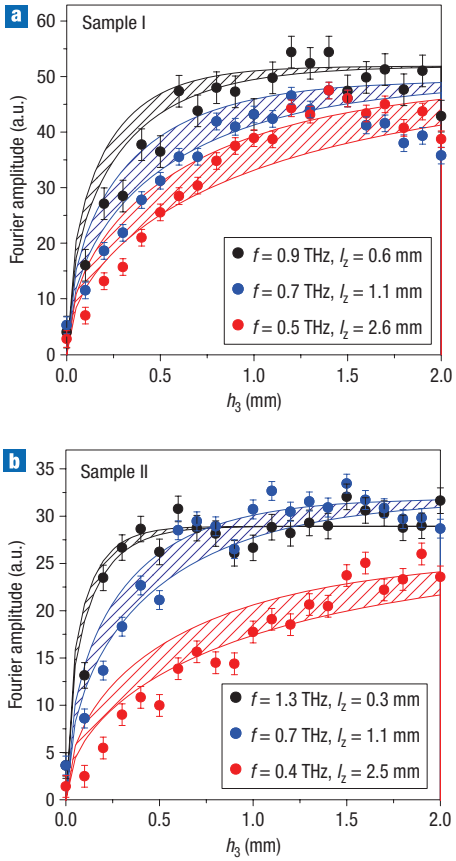

Figure 5 Experimental (points) and theoretical (shaded bands) electric-field amplitudes as a function of h_3. The error bars denote uncertainties in experimental measurement, and the theoretical curves are represented as bands to reflect the uncertainty in geometrical sample parameters, and are evaluated from equation (1) using the MEA. **a**, Data for sample I at $f = 0.9$, 0.7 and 0.5 THz. **b**, Data for sample II at $f = 1.3$, 0.7 and 0.4 THz.

technique (FIT) in the perfect-conductor approximation. Figure 4a–c shows the distribution of the electric field evaluated in the x–z plane of sample II for three different values of h_3. The aperture dimensions and positions are the same as experiment. The output coupler is located at the right-hand edge of the structure displayed and is not shown. The frequency of the incident radiation (1.3 THz) is close to the zone boundary where large confinement of the SPP is expected. It is clear from Fig. 4a–c that the intermediate razor blade selectively passes the SPP while blocking unwanted radiation diffracted at the input coupler. In Fig. 4d, several z-cuts along the propagation direction showing the decay of the SPP field in Fig. 4b ($h_3 = 0.5$ mm) are presented to allow comparison of the field confinement within and after the intermediate aperture. The field profile is maintained during the transmission process and the decay of the SPP in the direction perpendicular to the surface closely corresponds to that calculated from the dispersion relation obtained using the MEA (Fig. 1b), as assumed in deriving equation (1).

We now verify that the dependence of the output signal on h_3 carries information on the spatial confinement of the SPP. In Fig. 4e, the ratio A_2/A_1 obtained using the FIT is compared with that evaluated using equation (1) and the dispersion relation obtained using the MEA (Fig. 1b) as a function of h_3 at 0.7 THz and 1.3 THz. The good agreement obtained between the FIT prediction, which includes diffraction at the aperture, and the quasi-analytical MEA predictions, which neglect it, makes us confident of the experimental technique's ability to probe the confinement of the SPP propagating at the surface of the metamaterial, at least for h_3 greater than of the order of the free-space wavelength. For smaller h_3, the SPP amplitude is underestimated because of diffraction. This comparison also shows that the condition assumed in the metamaterials concept—that d and the aperture edge length, a, must be much less than the wavelength, λ—is quite relaxed in practice.

The experimental variation of $E(\omega)$ with h_3 for the two samples is shown in Fig. 5, which also shows theoretical predictions based on equation (1) with k_z evaluated using MEA and scaled vertically to fit the data. The corresponding theoretical values for l_z are tabulated in the figure. The agreement between theory and the measured amplitudes appears very good, particularly for the higher frequencies where the confinement is strongest and diffraction is weakest, and for aperture heights of the order or greater than the free-space wavelength, as anticipated from the above discussion. A fitting of the complete datasets (including the smallest aperture height) to equation (1) overestimates the decay length by a factor of the order of two for the reasons discussed, and for signal-to-noise ratio reasons it is not possible to restrict the fitted data to large h_3. A more accurate experimental determination of l_z requires either a near-field probing scheme avoiding diffraction, or an analytical treatment that takes diffraction into account. It is, however, clear that wavelength-scale energy confinement of the SPP over a wide frequency range near the band edge is experimentally observed, and that the degree of confinement is in close agreement with theory when account is taken of the approximations inherent in equation (1).

In conclusion, on our metamaterial surfaces we observe wavelength-scale energy confinement over the octave below the zone boundary, two orders of magnitude better than for a flat metal sheet and in agreement with theoretical predictions. We have not measured the propagation loss, but it should be proportional to l_z^{-2} if metal absorption dominates over diffraction. From a comparison with the theory of Zenneck waves on copper, the amplitude decay length l_x is estimated to be of the order of 5 cm near the band edge for our structures, reflecting a tolerable trade-off between loss and confinement. These characteristics are very encouraging for future applications in chemical or biochemical sensing, particularly as the vertical confinement can be increased by almost one order of magnitude by filling the holes with a high-index dielectric such as silicon. This would allow access to the flat part of the SPP dispersion relation, and spatial variation of the hole size or period could be used to create optical elements such as waveguides, lenses, mirrors and resonant cavities.

METHODS

DEVICE FABRICATION

Samples were fabricated by copper plating of lithographically patterned polymer films. A thin layer of SU8-5, an epoxy-based photoresist, was initially spun on to silicon wafers to create a base layer. A 60-μm-thick layer of SU8-50 was then applied and patterned with arrays of holes using contact optical lithography. Copper was deposited on the cured SU8 surfaces by catalytic plating using the Shipley Circuposit electroless process. Sample I had a period $d = 150$ μm and hole edge $a = 91 \pm 5$ μm, and sample II had $d = 100$ μm and $a = 66 \pm 4$ μm. The hole depth in each sample was 58 ± 6 μm, and the copper thickness was ~0.5 μm. The uncertainties reflect systematic variations across the samples associated with the fabrication technique and the existence of undercut in the hole side-wall (see Fig. 2). The samples were 40 mm long and 8 mm wide.

TECHNIQUES

Experiments were carried out using photoconducting THz sources and emitters described previously[27]. Pulses of 100 fs duration at a centre wavelength of 755 nm were used to optically excite a region of high electric field between electrodes deposited on semi-insulating GaAs. Terahertz radiation emitted by the transient photocurrents was collimated and refocused using a combination of hyper-hemispherical substrate lenses and off-axis parabolic mirrors before being detected by a 10-μm-long photoconducting dipole antenna. The receiver was optically gated by a second, time-delayed optical pulse split off from the first. By varying the time delay between these pump and probe pulses, which were delivered using photonic-crystal fibre, the electric field could be effectively mapped out as a function of time with a useful system bandwidth exceeding 2 THz. The $1/e$ diameter of the THz beam on the in-coupling aperture was $\sim$2 mm at 1 THz. Broadband phase-matching of free-space radiation and SPPs was achieved by exploiting diffraction to provide larger wavevectors parallel to the surface[16,28]. Experimentally, we found that the small sample width perpendicular to the SPP propagation direction did not affect our results as long as the centre of the incident THz beam was positioned within 2 mm of the long central axis of the sample. The screen (see Fig. 2), which was made from a THz absorbing, graphite-loaded polymer, prevented radiation scattered from the edge of the sample from reaching the detector. The aperture widths $h_1 = h_2$ were experimentally chosen to maximize the SPP signal amplitude and were 100 μm and 200 μm for samples I and II, respectively. The amplitude coupling efficiency at each aperture was $\sim$10%. The SPP signal was small but finite when h_3 was nominally zero because of a slight curvature of the sample surfaces.

Finite-integration technique calculations were performed using Microwave Studio (CST, Germany).

Received 13 September 2007; accepted 20 December 2007; published 3 February 2008.

References

1. Smith, D. R., Pendry, J. B. & Wiltshire, M. C. K. Metamaterials and negative refractive index. *Science* **305,** 788–792 (2004).
2. Pendry, J. B., Holden, A. J., Robbins, D. J. & Stewart, W. J. Magnetism from conductors and enhanced nonlinear phenomena. *IEEE Trans. Microwave Theory Tech.* **47,** 2075–2084 (1999).
3. Pendry, J. B., Holden, A. J., Stewart, W. J. & Youngs, I. Extremely low frequency plasmons in metallic meso structures. *Phys. Rev. Lett.* **76,** 4773–4776 (1996).
4. Pendry, J. B., Martin-Moreno, L. & Garcia-Vidal, F. J. Mimicking surface plasmons with structured surfaces. *Science* **305,** 847–848 (2004).
5. Shah, J. *Ultrafast Spectroscopy of Semiconductors and Semiconductor Nanostructures* (Springer, New York, 1996).
6. Ferguson, B. & Zhang, X.-C. Materials for THz science and technology. *Nature Mater.* **1,** 26–33 (2002).
7. Strachan, C. J. *et al.* Using terahertz pulsed spectroscopy to quantify pharmaceutical polymorphism and crystallinity. *J. Pharm. Sci.* **94,** 837–846 (2005).
8. Nagel, M. *et al.* Integrated THz technology for label-free genetic diagnostics. *Appl. Phys. Lett.* **80,** 154–156 (2002).
9. Yamamoto, K. *et al.* Noninvasive inspection of C-4 explosive in mails by terahertz time-domain spectroscopy. *Jpn J. Appl. Phys.* **43,** L414–L417 (2004).
10. Zhang, J. & Grischkowsky, D. Waveguide terahertz time-domain spectroscopy of nanometer water layers. *Opt. Lett.* **29,** 1617–1619 (2004).
11. Kurt, H. & Citrin, D. S. Coupled-resonator optical waveguides for biochemical sensing of nanoliter volumes of analyte in the terahertz region. *Appl. Phys. Lett.* **87,** 24119–241121 (2005).
12. Maier, S. A. *Plasmonics—Fundamentals and Applications* (Springer, New York, 2007).
13. O'Neal, D. P., Hirsch, L. R., Halas, N. J., Payne, J. D. & West, J. L. Photothermal tumor ablation in mice using near infrared absorbing nanoshells. *Cancer Lett.* **209,** 171–176 (2004).
14. Barnes, W. L., Dereux, A. & Ebbesen, T. W. Surface plasmon subwavelength optics. *Nature* **424,** 824–830 (2003).
15. Ozbay, E. Plasmonics: Merging photonics and electronics at nanoscale dimensions. *Science* **311,** 189–193 (2006).
16. Saxler, J. *et al.* Time-domain measurements of surface plasmon polaritons in the terahertz frequency range. *Phys. Rev. B* **69,** 155427 (2004).
17. Wang, K. & Mittleman, D. M. Metal wires for terahertz waveguiding. *Nature* **432,** 376–379 (2004).
18. Jeon, T.-I. & Grischkowsky, D. THz Zenneck surface wave propagation on a metal sheet. *Appl. Phys. Lett.* **88,** 061113 (2006).
19. Gómez-Rivas, J., Kuttge, M., Haring Bolivar, P., Kurz, H. & Sánchez-Gil, J. A. Propagation of surface plasmon polaritons on semiconductor gratings. *Phys. Rev. Lett.* **93,** 256804 (2004).
20. Goubau, G. Surface waves and their application to transmission lines. *J. Appl. Phys.* **21,** 1119–1128 (1950).
21. Mills, D. L. & Maradudin, A. A. Surface corrugation and surface-polariton binding in the infrared frequency range. *Phys. Rev. B* **39,** 1569–1574 (1989).
22. Ulrich, R. & Tacke, M. Submillimeter waveguiding on periodic metal structure. *Appl. Phys. Lett.* **22,** 251–253 (1973).
23. Hibbins, A. P., Evans, B. R. & Sambles, J. R. Experimental verification of designer surface plasmons. *Science* **308,** 670–672 (2005).
24. Garcia-Vidal, F. J., Martin-Moreno, L. & Pendry, J. B. Surfaces with holes in them: New plasmonic metamaterials. *J. Opt. A* **7,** S97–S101 (2005).
25. Maier, S. A. & Andrews, S. R. Terahertz pulse propagation using plasmon-polariton-like surface modes on structured conductive surfaces. *Appl. Phys. Lett.* **88,** 251120 (2006).
26. Jepsen, P. U., Jacobsen, R. H. & Keiding, S. R. Generation and detection of terahertz pulses from biased semiconductor antennas. *J. Opt. Soc. Am. B* **13,** 2424–2436 (1996).
27. Andrews, S. R., Armitage, A., Huggard, P. G. & Hussain, A. Optimization of photoconducting receivers for THz spectroscopy. *Phys. Med. Biol.* **47,** 3705–3710 (2002).
28. Zhizhin, G. N., Moskalova, M. A., Shomina, E. V. & Yakovlev, V. A. *Surface Polaritons: Electromagnetic Waves at Surfaces and Interfaces* (eds Agranovich, V. M. & Mills, D. L.) (North Holland, Amsterdam, 1982).

Acknowledgements

This work was supported by the Air Force Office of Scientific Research (AFOSR) (FA9550-05-1-0488) and the Royal Society. Financial support from the Spanish Ministerio de Educación y Ciencia (MEC) under contract MAT2005-06608-C02 and from the EU under project FP6-2002-IST-1-507879 (Plasmo-Nano-Devices) is also gratefully acknowledged.
Correspondence and requests for materials should be addressed to S.A.M. or F.J.G.-V.